Self-assembled materials and devices that process light

Peiwang Zhu[a], Hu Kang[a], Milko E. van der Boom[a†], Zhifu Liu[b],
Guoyang Xu[b], Jing Ma[b], Delai Zhou[b], Seng-Tiong Ho[b], and Tobin J. Marks[a*]

[a] Department of Chemistry and Materials Research Center,
Northwestern University, Evanston, IL 60208-3113
[b] Department of Electrical and Computer Engineering and Materials Research Center,
Northwestern University, Evanston, IL 60208-3113

ABSTRACT

Self-assembled superlattices (SASs) are intrinsically acentric and highly cross-linked structures. For organic electro-optics, they offer great advantages such as not requiring electric field poling for creating an acentric, EO-active microstructure and having excellent chemical, thermal, and orientational stabilities. In this paper, a greatly improved two-step all "wet-chemical" self-assembly (SA) approach is reported. Excellent radiation hardness of the SAS films is demonstrated by high-energy proton irradiation experiments. By introducing metal oxide nanolayers during SA, we show that the refractive indices of SAS films can be tuned over a wide range. Through special chromophore design, the optical absorption maxima of SAS films can also be greatly blue-shifted. Prototype waveguiding electro-optic modulators have been fabricated using the SAS films integrated with low-loss polymeric materials functioning as partial guiding and cladding layers. EO parameters such as the half-wave voltage and the effective electro-optic coefficient are reported.

Keywords: Self-assembled superlattice (SAS), electro-optic (EO) material, EO modulator, charge-transfer band, blue shift.

1. INTRODUCTION

The formation of functional nanoscale multimolecular organizates and the efficient translation of molecular properties into macroscopically observable responses are topics of great current interest.[1-5] A high level of structural control at nanoscale dimensions is a necessary requirement to exert full control over numerous materials properties (such as optoelectronic, electrical, magnetic, etc.). Many factors at the molecular level (e.g., molecular architecture and electronic structure, reactivity, electrostatics, hydrogen-bonding, van der Waals interactions, etc.) play an essential role in the design and build-up of structures with elaborate architectural complexity. Crystal engineering,[3] Langmuir-Blodgett (LB) film deposition,[4] as well as self-assembly (SA) and self-organization,[1,5] are only a few of many contemporary examples of rational approaches to amplifying molecular properties and inducing order and intermolecular communication in condensed soft matter. In this regard, the formation of device-quality molecular photonic materials represents a promising direction in the quest to obtain greater spatial and temporal control over light wave propagation in the solid state. Molecular electro-optic materials offer a particular synthetic challenge since organizing large-hyperpolarizability (hence dipolar) chromophoric building blocks into *acentric microstructures* presents large thermodynamic challenges.[6-8] Nevertheless, great progress has been made using electric field poling of glassy polymers,[9-11] Langmuir-Blodgett film growth,[4] and the self-assembly of covalently interconnected superlattices.[12-16] In addition to fundamental scientific drivers, the successful creation of large-response molecular assemblies with acceptable transparency, robustness, and processing properties could lead to novel low switching voltage/large bandwidth electro-optic (EO) light modulators and related devices, promising greatly increased rates of information transmission by enhancing speed, capacity, and bandwidth for optical data telecommunications and networking.

For all these reasons, development of efficient synthetic methodologies for the growth and modification of structurally elaborate photonically/electronically functional superlattices with excellent optical, thermal, and chemical properties is of great scientific interest and potential utility. Among the aforementioned stratagies, layer-by-layer siloxane-based SA offers many advantages: i) SASs offer higher EO coefficients and lower dielectric constants than established inorganic materials (e.g., LiNbO$_3$); ii) The chromophores are covalently linked to the substrates, and the films are closely packed and robust. Molecular orientation is intrinsically acentric, and post-deposition processing steps

---

[†] Present address: Department of Organic Chemistry, The Weizmann Institute of Science, Rehovot, 76100, Israel.
[*] To whom correspondence should be addressed. Email: t-marks@northwestern.edu. Phone: 1 847 4915658.

such as poling are not necessary; iii) Chromophore orientation is locked into place with strong covalent Si-O bonds, hence the microstructural orientation is very stable; iv) Precise control of film refractive index can be achieved at the sub-wavelength molecular level; v) Absorption bands can be tuned by implanting quantum chemically designed building blocks; vi) Large area films can be easily prepared; vii) Chromophore arrays can be fabricated on silicon or a variety of related substrates, allowing ready device integration and therefore significantly reduced device design complexity.

In this contribution, we briefly report recent progress in this laboratory on: 1) efficient self-assembly through an all "wet-chemical" approach; 2) tuning the refractive indices of self-assembled EO films; 3) SAS radiation hardness; 4) ultra blue-shifted SA materials; 5) EO device design and fabrication.

2. SELF-ASSEMBLED EO MATERIALS

2.1 Efficient self-assembly through an all "wet-chemical" approach

Previous studies in this lab developed a three-step procedure to fabricate robust, acentric multilayer superlattices composed of stilbazolium and related chromophores, and exhibiting very large NLO / EO responses ($\chi^{(2)}$ =150-200 pm/V). Devices such as ultrafast frequency-selective switching devices, TE mode EO-phase modulators, and frequency doubling devices have been fabricated with these SAS materials.[17-18] These results stimulated our interest in broadening and refining layer-by-layer deposition processes for EO film growth. Since the thickness required for optimum single mode waveguiding EO film devices should be ~ 0.5 μm or more, at least 150 SAS trilayers (450 growth steps) are required for this three-step procedure. Therefore, to be practical, the procedure should be automated and should equal or surpass other well-established layer-by-layer growth techniques (e.g., LB methods) in terms of film growth efficiency, microstructural regularity, and growth flexibility. In the three-step "first-generation" procedure,[13] a coupling layer is first self-assembled onto the substrate. Secondly, the chromophore is linked covalently to the coupling layer through a quaternization reaction. Thirdly, a planarizing capping layer is deposited. However, since the quaternization reaction is very slow, spin-coating followed by 110 °C vacuum oven treatment is necessary to obtain full chromophore coverage. This step is a serious deficiency in automating the growth process.

A greatly improved all-"wet-chemical" self-assembly approach[19] to these large-response optically/electronically functional siloxane-based SAS films has recently been developed using reactive –SiCl$_2$I derivatives of a protected azobenzene chromophore and a chlorosiloxane deprotecting/capping reagent (**Scheme 1**). The deposition technique reported here employs the iterative combination of *only two steps*: (i) Self-limiting polar chemisorption of a protected high-β chromophore (*4-(4-{bis-[2-(tert-butyl dimethyl silanyloxy)-ethyl]-amino}-phenylazo)-1-[4-(dichloro-iodo-silanyl)-benzyl]pyridinium iodide (**PAPI**, **Scheme 1**) monolayer (*t* ~15 min.), and (ii) *in situ* trialkylsilyl group removal and self-limiting capping of each chromophore layer using octachlorotrisiloxane (*t* ~25 min.; **Scheme 1**). This latter step deposits a robust polysiloxane layer which stabilizes the polar microstructure via interchromophore crosslinking and simultaneously regenerates a reactive hydrophilic surface.
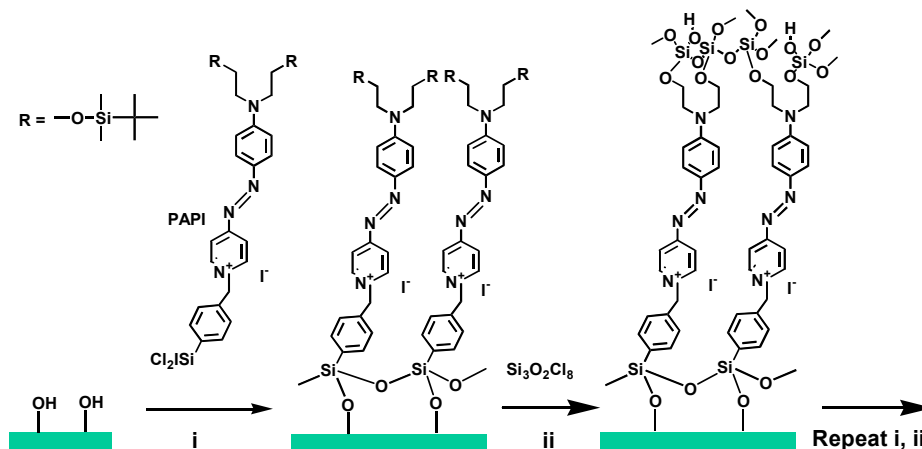
Scheme 1. Schematic representation of the two-step layer-by-layer self-assembly of self-assembled superlattices.

UV-vis measurements unambiguously reveal a linear dependence of the HOMO-LUMO chromophore optical CT absorbance at λ = 575 nm on the number of bilayers, demonstrating that essentially equal quantities of uniformly aligned chromophore units are incorporated in each sublayer up to 40 bilayers (**Figure 1**). No other bands or shifts in the optical absorbance maxima are observed, arguing against significant chromophore aggregation or decomposition. Polarized transmission SHG measurements on the present SAS structures at λ_o = 1064 nm were carried out on SAS samples placed on a computer-controlled rotation stage, enabling the incidence angle of the input radiation to the sample surface normal to be varied from 0° to 70°. Angle-dependent SHG interference patterns for glass substrates coated on both sides with SAS films demonstrate that the two-step deposition process affords identical film quality and uniformity on both sides of the substrate (**Figure 2**; inset). The approximately quadratic dependence of the absorption-corrected $I^{2\omega}$ on the number of bilayers (**Figure 2**) indicates the preservation of a polar microstructure as the layer-by-layer assembly progresses.
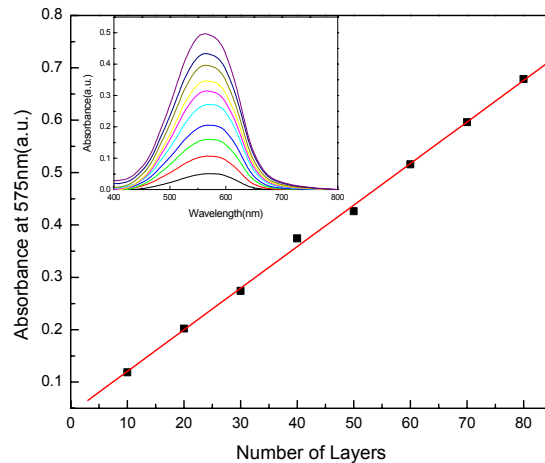

Figure 1. Optical absorption spectra of SAS films at 575 nm as a function of the number of **PAPI**-based layers. The solid line is the fit by linear regression. **Inset:** UV-vis absorption spectra of 4, 8, 12 ⋯⋯ and 40 layers samples.
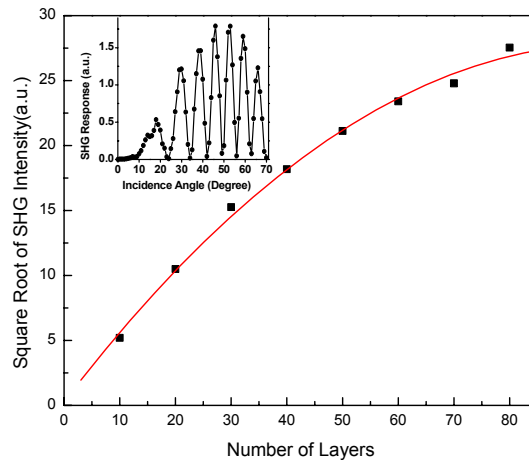

Figure 2. Absorption corrected square-root of SAS 532 nm SHG response ($I_{corrected}{}^{2\omega}$) as a function of the number of **PAPI**-based layers. **Inset:** SHG response as a function of fundamental beam incident angle from a float glass slide having a SAS layer on either side. The solid line is drawn as a guide to the eye.

This two-step, layer-by-layer approach yields thermally robust SAS films exhibiting large NLO/EO responses ($\chi^{(2)}$ ~180 pm/V, r_{33} ~65 pm/V at 1064 nm) and can be efficiently carried out in a single reaction vessel using standard cannula techniques or by consecutive substrate dipping in a nitrogen-filled glovebag. Since only "wet-chemical"

processes are involved, it is easy to automate. The film assembly time is now comparable to LB and other layer-by-layer deposition techniques, thus offering an efficient route to thicker self-assembled EO films.

2.2 Tuning SAS refractive indices

In a typical EO modulator, the EO-active chromophore layer is generally sandwiched between two cladding layers. One of the basic requirements is that the refractive index of the EO active layer must be greater than that of the cladding layers so that the propagating light can be effectively confined in the EO-active layer. Organic EO materials with greater refractive indices are therefore desired so that there will be wider choices for cladding materials. Unfortunately, the refractive indices of most organic materials are not particularly large, and are not tunable for specific materials. However, for the layer-by-layer SA materials, it is relatively straightforward to introduce various metal oxides layers to increase the refractive index. **Scheme 2** shows an example. This one-pot all wet-chemical approach involves: (i) layer-by-layer covalent self-assembly of intrinsically acentric multilayers of high-hyperpolarizability chromophores, (ii) protecting group cleavage to generate a hydrophilic surface, (iii) self-limiting capping of each chromophore layer with octachlorotrisiloxane, (iv) deposition of metal oxide nanolayers derived from THF solutions. of $Ga(O^iPr)_3$ or $In(O^iPr)_3$, and (v) covalent capping of the resulting superlattices. Microstructurally regular acentricity and sizable electrooptic responses are retained in this straightforward synthetic procedure.[20] The intercalation of metal oxide components into the SAS microstructures significantly increases the refractive indices of the films. Thus, refractive indices of n = 1.76 (Ga) and n = 1.84 (In) at 650 nm are determined for these films by spectroscopic ellipsometry. These values are substantially greater than that of the metal-free SAS-films where n = 1.52 at 650 nm. Dispersion data are shown in **Figure 3**.
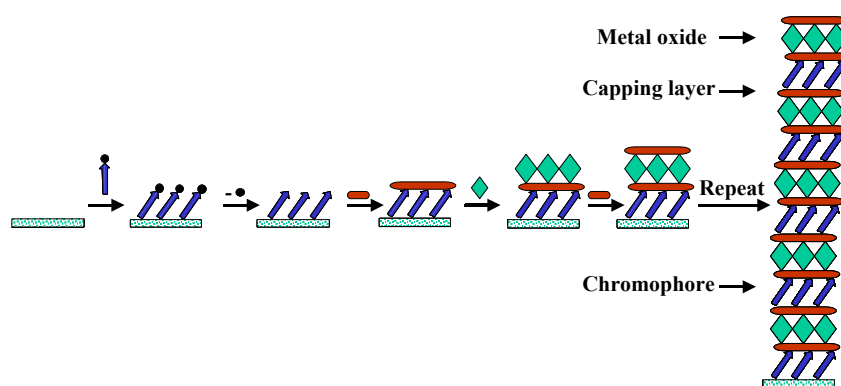
Scheme 2. Layer-by-layer SAS growth with incorporation of metal oxide nanolayers growth process for refractive index tuning.
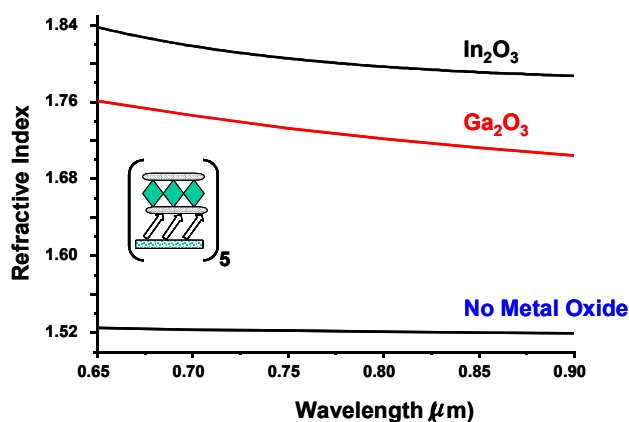

Figure 3. Ellipsometry-derived refractive indices of Ga_2O_3, In_2O_3, and "all-organic" **PAPI**-based SAS films.

2.3 Stability of SAS against proton radiation

Since the SAS microstructure is highly cross-linked, it is very stable. The films have excellent mechanical strength and excellent chemical resistance. Thus they cannot be detached in the standard Scotch tape decohesion test and are stable against common organic solvents such as acetone, chloroform, alcohol, etc. This is a great advantage for further device processing. Moreover, since the chromophore dipoles are locked into place by the capping reagent, the polar orientation is intrinsic and does not decay with time. One potential application for SAS materials might be in satellite communication, where chemical and orientation stabilities are critical. To simulate the space environment, two samples were irradiated with high-energy protons. The samples were prepared on float glass by the two-step SA methodology described in **Scheme 1** with 22 or 24 bilayers deposited on both sides. Both samples were fully characterized using UV-vis and SHG spectroscopy before irradiation. Proton irradiation was then conducted at the Crocker Nuclear Laboratory (CNL, UC Davis). Samples were irradiated for varying times with 61 MeV protons. These energies are representative of trapped protons for the low earth orbit (LEO, 1000 km from earth, 55° inclination) and the middle earth orbit (MEO, 10000 km from earth, 55° inclination) type missions. The UV-vis spectra of these samples after irradiation are found to be identical to those prior to irradiation. Furthermore, **Table 1** shows a comparison of SAS film SHG response before and after irradiation. No significant decay is observed, meaning that the SAS materials should be quite stable to space radiation over 100 (for LEO) and 200 (for MEO) years.

Table 1. Comparison of SAS film SHG response before and after proton radiation.

| Sample	Radiation Dose (Krad(Si))	Equivalent Mission Duration in Years at LEO	Equivalent Mission Duration in Years at MEO	$(I_s^{(2\omega)}/I_q^{(2\omega)})^{1/2}$ SHG response vs. quartz
1	0	0	0	0.113
	91.4	50	119	0.117
2	0	0	0	0.130
	182.7	100	238	0.127

2.4 SAS materials with ultra blue-shifted optical absorption

Conventional large-β EO chromophores are typically one-dimensional (1D) planar, long conjugation length π systems end-capped with donor and acceptor (D, A) moieties. These materials usually exhibit intense low-lying longitudinal charge-transfer (CT) absorptions. Considerable, elegant efforts have worked to increase β by optimizing D/A strengths and/or the conjugation pathways of such 1D chromophores.[6-11] However, implicit in this approach is the challenge of optimizing the nonlinearity-transparency tradeoff in which increases in β for such chromophores are almost invariably accompanied by bathochromic shifts of the optical maximum. Furthermore, molecules with such extended π systems and low-lying excited states are frequently have poor chemical and thermal stability. Alternative molecular design strategies would therefore be desirable. To this end, non-traditional NLO chromophores with multiple donor-acceptor substitutents have attracted recent attention, ranging from dipolar "X-shaped"[21] and "Λ-shaped"[22] to octopolar molecules.[23] It is known that multiple D,A substitution affords chromophore 2D character in which off-diagonal β tensor components become significant, offering among other features, possible relaxation of nonlinearity-transparency tradeoffs and improved phase-matching via the larger off-diagonal components.[24] However, few experimental studies of two-dimension (2D) dipolar EO chromophores have been reported, with most examples exhibiting modest hyperpolarizabilities as a consequence of short conjugation lengths, with only a few being incorporated in LB or poled polymer thin films.[21,24]

A novel type of "X-shaped" 2D chromophore having an aromatic central core fused to extended, conjugated D/A tetrasubstitution was recently developed in this laboratory. The optical transition dipoles couple so as to drastically blue-shift λ_{max} while maintaining a very large β response. The blue-shifted X chromophore HOMO-LUMO CT excitation can be explained in terms of the excitonic transition dipole coupling, leading to a first excited state composed of a pair of excitonic states. The upper excitonic state is optically allowed, and optical transitions from the ground state populate the upper excitonic state, resulting in a spectral blue shift. In the X chromophore, *intramolecular* coupling of transition

dipoles in 2D is sufficiently strong as to produce a dramatically blue-shifted optical maximum. This chromophore was specifically designed for a covalent layer-by-layer siloxane self-assembly (SA) approach to afford polar, robust, and structurally regular thin films. To our knowledge, this is the first example of blue-shifted chromophore incorporation in such a SA approach.

The chromophore precursor 1,2-bis-((*E*)-2-pyridin-4-yl-vinyl)-4,5-bis{(*E*)-2-[*p-N,N*-bis(2-tert-butyldimethylsiloxyethyl)amino-phenyl]ethenyl}-benzene (**BPBAB**) was synthesized via a sequence of Wittig-Horner and Heck coupling reactions (**Scheme 3**). The dicationic methylpyridinium X chromophore (**X-CHR**) was then obtained via alkylation of **BPBAB** with MeOTf. All new compounds were characterized by conventional analytical/spectroscopic methodologies. More details will be reported elsewhere.[25] Thermal analysis data show that both **BPBAB** and **X-CHR** have excellent thermal stability ($T_d \approx 340°C$ for **BPBAB** and $T_d \approx 280°C$ for **X-CHR**).
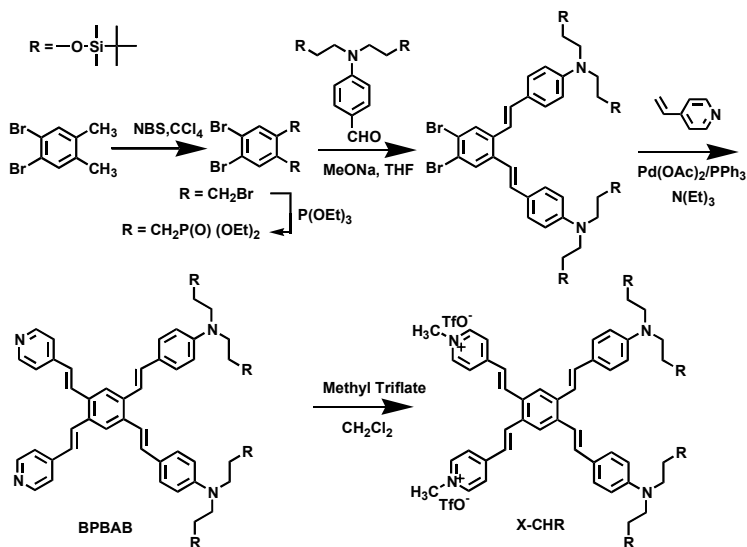
Scheme 3. Synthesis of X-shaped chromophore (**X-CHR**).

The **X-CHR** optical spectrum (**Figure 4**) in CH_2Cl_2 solution consists of an intense band centered at 357 nm ($\varepsilon = 12000$ L mol^{-1} cm^{-1}) involving $\pi \rightarrow \pi^*$ CT and a less intense, broad band at 440-700 nm, responsible for the red color, and associated with aggregation as supported by concentration-dependent optical absorption spectra ($5 \times 10^{-7} \rightarrow 3 \times 10^{-8}$ M), which reveal an increase of the 357 nm CT band and diminution of the long-λ band upon dilution. This tendency for aggregation is also seen in concentration-dependent NMR experiments.[25]
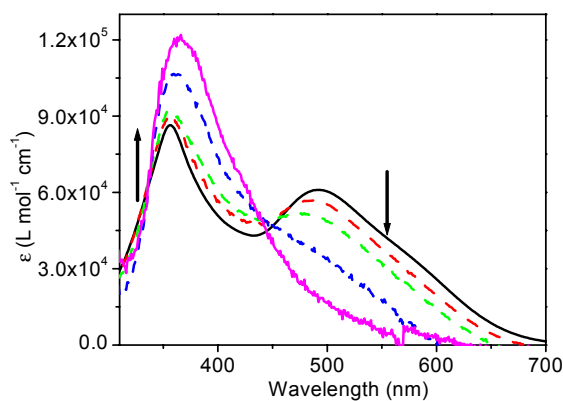

Figure 4. Concentration-dependent optical absorption spectra of chromophore **X-CHR** in CH_2Cl_2 solution. The arrows indicate changes of the monomer aggregation bands upon dilution from 5×10^{-7} to 3×10^{-8} M.

Layer-by-layer self-assembled X chromophore thin films were grown via an iterative three-layer process (**Scheme 4**): (i) self-limiting chemisorption of $4\text{-}Cl_2ISiC_6H_4CH_2I$ onto a hydrophilic substrate surface; (ii) SA of chromophore precursor **BPBAB** onto the benzyl halide-functionalized substrate via quaternization; and (iii) $Cl_3SiOSi(Cl_2)OSiCl_3$ capping to planarize/crosslink the polar structure and regenerate an active surface for deposition of subsequent layers. The resulting SAS films exhibit λ_{max} at the remarkably short wavelength maximum of 325 nm (**Figure 5**). The additional blue-shifting of the film λ_{max} vs. solution is consistent with *intermolecular* dipole-dipole coupling in the closely packed chromophore layers, where strong π-π interactions are possible. The linear dependence of the 325 nm absorbance on the number of layers indicates that essentially identical quantities of equivalently oriented chromophore molecules are deposited in growing each layer. Polarized transmission SHG measurements at $\lambda_o = 1064$ nm demonstrate further that essentially identical film quality and uniformity are achieved on both sides of the substrates during growth. The quadratic dependence of the 532 nm output intensity ($I^{2\omega}$) on film thickness additionally demonstrates polar microstructure preservation as layer-by-layer self-assembly progresses. These films exhibit large second-order *non-resonant* macroscopic NLO responses $\chi^{(2)} \sim 232$ pm/V at 1064 nm converting to an estimated EO coefficient $r_{33} \sim 43$ pm/V at 1550 nm.[26]
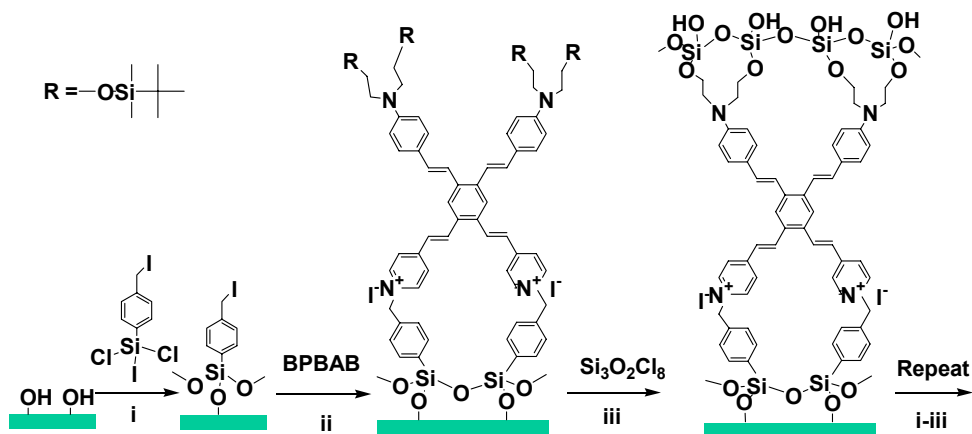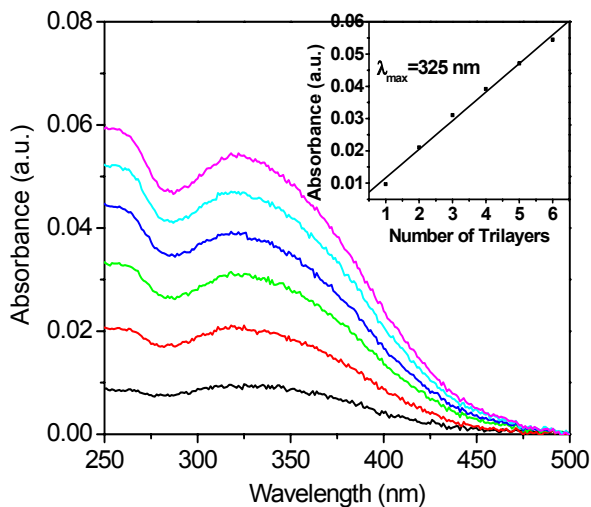

Scheme 4. Self-assembly of the X chromophore.

Figure 5. Optical absorption spectra of X-chromophore SAS films grown on fused quartz. **Inset**: optical absorbance of films at $\lambda_{max} = 325$ nm as a function of the number of layers.

3. EO DEVICE DESIGN AND FABRICATION

3.1 EO modulator device design

Using SAS thin films grown by the expeditious two-step process of **Scheme 1**, EO modulators were fabricated. The cross-section of a typical ridge waveguide is shown in **Figure 6**, with the bottom electrode located under the lower cladding layer, and the top electrode above the top cladding layer. The optical modes propagating in the waveguide may be calculated by the beam propagation method (BPM). As a good estimation, in order to find the single mode condition for the ridge waveguide, the ridge waveguide is divided into a central region (region **II**) and two lateral regions (regions **I** and **III**). For each of the three regions, an approach was used that treats the region as a multilayer planar waveguide, and transfer matrices were applied that connect adjacent layers.[27] Effective TE (or TM) mode refractive indices may be obtained for each region. The resultant effective indices for the three regions were used as TM (or TE) refractive index parameters of a symmetric three-layer waveguide having guiding layer thickness t_g.[28] The thickness of the cladding layers was chosen so that the loss induced by the metal electrodes was less than 0.5 dB/cm. **Figure 7** shows the computed bottom metal loss versus the core layer thickness of an EO modulator with a 1.4 µm top cladding layer of CYTOP.
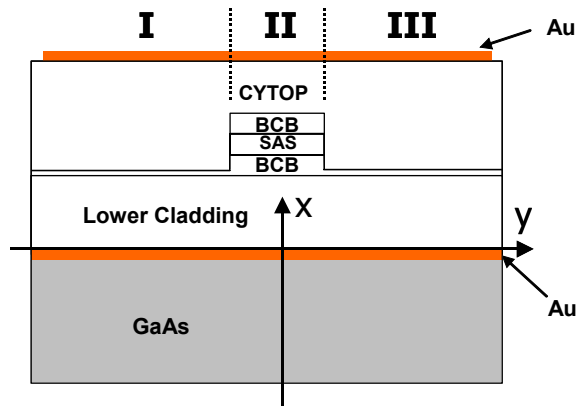

Figure 6. Cross-section of a waveguiding EO modulator based on SAS thin films integrated with the polymers BCB and CYTOP on a GaAs wafer coated with a SiO$_2$ layer.
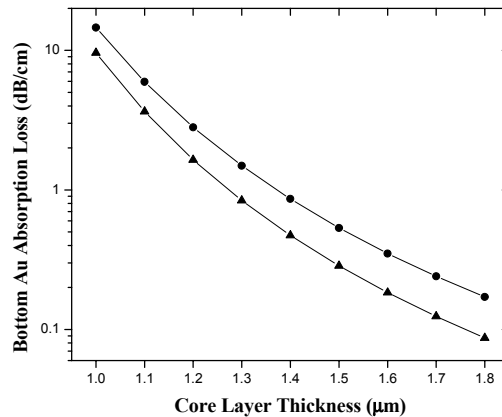

Figure 7. Simulated bottom metal absorption loss versus waveguide core layer thickness for the device shown in Figure 6. Dots and solid triangles correspond to 2.5 µm and 2.7 µm thick SiO$_2$ bottom cladding layers, respectively. The top cladding layer of CYTOP is 1.4 µm thick.

3.2 EO modulator fabrication

The EO waveguide modulator configuration shown in **Figure 6** has a five-layer stack structure and was fabricated using a multistep process including E-beam evaporation, plasma-enhanced chemical vapor deposition (PECVD), spin-coating and curing, superlattice self-assembly, photolithography, reactive ion etching (RIE), and metal deposition and lift-off techniques. The polymer CYTOP (from Asahi Glass Co., c/o Bellex International Corp., Wilmington, DE 19809) was used for the upper cladding layer, while SiO_2 functions as the lower cladding layer. In the waveguide structure, the SAS layer combined with layers of the polymer BCB (from Dow Chemical Co., Midland, MI 48674) served as the guiding layer. The refractive index of BCB ($n \sim 1.54$ at a wavelength of 1064 nm) is close to that of the SAS films, and the refractive index of CYTOP is 1.34 at 1064 nm. Both CYTOP and BCB exhibit good optical transparency over a wide wavelength range from the UV to infrared.

In order to achieve good adhesion between the substrate and Au bottom electrode, a thin layer of TiW (about 10 nm) was deposited prior to the deposition of the gold electrode. Gold (200 nm thick) was deposited by sputtering or e-beam evaporation. The SiO_2 cladding layer (about 2.5 μm) was then deposited on the gold by a PECVD process. A layer of the polymer BCB was then spin-coated on the SiO_2 layer. It was fully cured in an oven under a nitrogen flow. Since the SAS can only be grown on hydrophilic surfaces, O_2 reactive ion etching (RIE) was used to treat the BCB surface. This ensures that ample hydroxyl groups are present for SAS growth. One hundred SAS layers were grown on the substrate using the approach described in **Scheme 1**. The thickness of the resulting SAS film is about 0.32 μm. A second layer of BCB was then spin-coated on the surface of the SAS layers and cured as described above. In order to reduce the loss due to the electrodes of the final waveguide, the thicknesses of both the BCB layers were chosen to be around 1.5 μm. BCB has a refractive index closely matched to that of the SAS material over a relatively broad wavelength range. The BCB/SAS/BCB triple layer structure functions as the guiding layer of the waveguide. A protective layer of CYTOP was then spin-coated on the top BCB layer and cured. Contact printing lithography and RIE processes were next used to fabricate ridge waveguide patterns on the polymer multilayer structure. CF_4 and O_2 gases were used for the RIE of the BCB and SAS layers respectively. Analysis and simulation showed that for given waveguide width (3.0 to 6.0 μm for one sample), a proper etching depth of the polymer layers may be chosen so as to allow the ridge waveguide to accommodate only a single optical mode. Another layer of CYTOP, functioning as the top cladding layer, was spin-coated onto the partially etched first CYTOP layer and cured. The top Au electrode (20-30 μm wide, and 0.25 μm in thickness) was then deposited using e-beam evaporation and lift-off techniques. The bottom electrode window was opened by a series of etching steps, including wet etching the top gold electrode, RIE etching the polymer layers, and wet etching the SiO_2 layer.

The thicknesses of the cladding and the guiding layers, and the RIE-derived ridge waveguide depths were estimated by using a Filmetrics optical profiler and SEM instrumentation. **Figure 8** shows an SEM image of the profile of a SAS-based electro-optic modulator, and an optical microscope image of the upper electrode patterns, respectively.
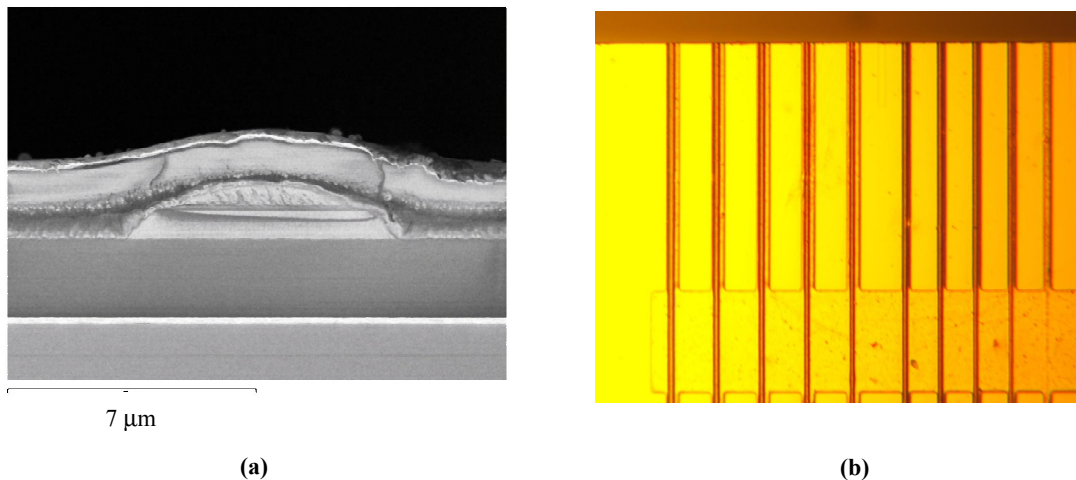

7 μm

(a)   (b)

Figure 8. (a) SEM cross-section image of an SAS-based electro-optic modulator, and **(b)** optical microscopic image of the upper electrode patterns.

3.3 Driving voltage measurements on the EO modulators

Figure 9 shows the setup for the measurement of the EO response of the present SAS-based waveguiding EO modulators. A diode pumped Nd:YAG laser operating at 1064 nm was used as the light source. The light was coupled into and out of the ridge waveguide using a pair of 40× microscope objectives. The device was operated by launching both TE and TM modes in the waveguide. The light beam propagates through a polarizer oriented at 45° with respect to the vertical direction before the objectives. The EO response was measured by end-firing the laser beam into one of the cleaved facets of the sample. Then the light went through an analyzer oriented perpendicular to the orientation of the polarizer. The modulated light signal was then coupled to a photodetector and monitored by an oscilloscope. **Figure 10** shows the typical EO response of a SAS-based EO modulator measured from the oscilloscope traces. In this figure, traces 1 and 2 represent the applied electrical signal and the response of the EO modulator, respectively. The half- wave voltage V_π was estimated to be about one hundred volts for the EO modulator sample shown. The effective EO coefficient r is related to the half-wave voltage V_π by $r = \dfrac{\lambda d}{n_{eff-opt}^{3} V_\pi L \Gamma}$, where λ is the wavelength of the optical wave, d the distance between the lower and the upper electrodes, $n_{eff\text{-}opt}$ the effective optical refractive index, L the length of the electro-optic interaction region, and Γ the overlap integral factor of the optical and the external electric fields,

$$\Gamma = \frac{d}{V} \frac{\iint E_e |E_o|^2 dxdy}{\iint |E_o|^2 dxdy} ,$$

where the E_e and E_o are the amplitudes of optical field, and external electric field under an applied voltage of V, respectively.
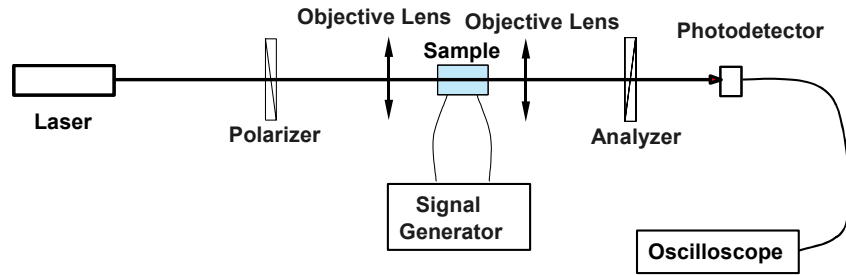
Figure 9. Setup for the measurement of the EO response of waveguiding EO modulators.
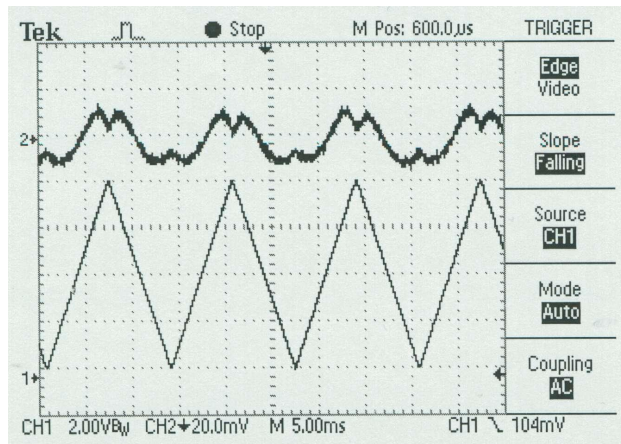
Figure 10. EO response from a prototype EO modulator based on a SAS thin film.

The effective EO coefficient r is estimated to be 23 pm/V. This value agrees well with that measured by a direct EO measurement setup for planar waveguide sample.[29] A longer waveguide (up to the cm level) and thicker SAS films (at the μm level) will help to achieve a much lower V_π.

4. CONCLUSIONS

Organic materials are promising candidates for fabricating fast EO modulators to use in future high bandwidth optical fiber communications. In this paper we described methods of fabricating and characterizing novel organic EO materials composed of self-assembled superlattices (SASs). These structures are intrinsically acentric and exhibit large second harmonic generation (SHG) and EO responses without the necessity of electric field poling with an external electric field. Excellent radiation hardness has been demonstrated by high-energy proton irradiation experiments. We also show that the refractive index can be broadly tuned by introducing metal oxide nanolayers during SA and that the absorption band can be drastically blue-shifted by using an "X-shaped" 2D charge-transfer chromophore. Prototype waveguide EO modulators have been fabricated using SAS films sandwiched between low-loss polymeric guiding and cladding layers having appropriate refractive indices. The waveguide EO modulators were fabricated using a multistep process including E-beam evaporation, PECVD, spin-coating and curing, superlattice self-assembly, photolithography, RIE, and metal deposition and lift-off techniques. The EO modulator parameters such as the half-wave voltage and the effective EO coefficient are also discussed.

ACKNOWLEDGMENTS

REFERENCES

1. J. F. Stoddart, *Acc. Chem. Res.*, **34**, 410-522(2002**). (**special issue on molecular machines).
2. J.-M. Lehn, *Supramolecular Chemistry*: *Concepts and Perspectives;* VCH: New York, 1995.
3. G. R.Desiraju, *Crystal Engineering: the Design of Organic Solids*: Elsevier: New York, 1989.
4. G. J. Ashwell; R. C. Hargreaves; C. E. Baldwin; G. S. Bahra; C. R. Brown, "Improved Second-Harmonic Generation from Langmuir-Blodgett Films of Hemicyanine Dyes"**,** *Nature*, **368**, 438-440(1994).
5. I. Weissbuch; P. N. W. Baxter; S. Cohen; H. Cohen; K. Kjaer; P. B. Howes; J. Als-Nielsen; G. S. Hanan; U. S. Schubert; J.-M. Lehn; L. Leiserowitz; M. Lahav, "Self-Assembly at the Air-Water Interface. In-Situ Preparation of Thin Films of Metal Ion Grid Architectures", *J. Am. Chem. Soc.*, **120**, 4850-4860(1998).
6. *Molecular Nonlinear Optics – Materials, Physics and Devices*; ed: Zyss, J.; Academic Press: San Diego, CA 1994.
7. *Chem. Rev.* special issue on "Optical Nonlinearities in Chemistry", ed: Burland, D. M., **94**, 1-278(1994).
8. L. Dalton, "Polymeric Electro-Optic Materials: Optimization of Electro-Optic Activity, Minimization of Optical Loss, and Fine-Tuning of Device Performance", *Opt. Eng.*, **39**, 589-595(2000).
9. J. D. Luo; M. Haller; H. Li; H.-Z. Tang; A. K.-Y. Jen; K. Jakka; C.-H. Chou; C.-F. Shu, "A Side-Chain Dendronized Nonlinear Optical Polyimide with Large and Thermally Stable Electrooptic Activity", *Macromolecules*, **37**, 248-250(2004).
10. F. Kajzar; K.-S. Lee; A. K.-Y. Jen, "Polymeric Materials and their Orientation Techniques for Second-Order Nonlinear Optics", *Adv. Poly. Sci.*, **161**, 1-85 (2003).
11. C. Ye; T. J. Marks; J. Yang; G. L. Wong, "Synthesis of Molecular Arrays with Nonlinear Optical Properties. Second-Harmonic Generation by Covalently Functionalized Glassy Polymers", *Macromolecules*, **20**, 2322-2324(1987).
12. R. Moaz; J. Sagiv, "Penetration-Controlled Reactions in Organized Monolayer Assemblies. 1. Aqueous Permanganate Interaction with Monolayer and Multilayer Films of Long-Chain Surfactants", *Langmuir*, **3**, 1034-1044(1987).

13. W. Lin; W. Lin; G. K. Wong; T. J. Marks, "Supramolecular Approaches to Second-Order Nonlinear Optical Materials. Self-Assembly and Microstructural Characterization of Intrinsically Acentric [(Aminophenyl)azo]pyridinium Superlattices", *J. Am. Chem. Soc.*, **118**, 8034-8042(1996).

14. S. Yitzchaik; T. J. Marks, "Chromophoric Self-Assembled Superlattices", *Acc. Chem. Res.*, **29**, 197-202(1996).

15. D.-Q. Li; M. A. Ratner; T. J. Marks; C.-H. Zhang; J. Yang; G. K. Wong, "Chromophoric Self-Assembled Multilayers. Organic Superlattice Approaches to Thin-Film Nonlinear Optical Materials", *J. Am. Chem. Soc.*, **112**, 7389-7390(1990).

16. M. E. van der Boom; P. Zhu; G. Evmenenko; J. E. Malinsky; W. Lin; P. Dutta; T. J. Marks, "Nanoscale Consecutive Self-Assembly of Thin-Film Molecular Materials for Electrooptic Switching. Chemical Streamlining and Ultrahigh Response Chromophores", *Langmuir*, **18**, 3704-3707(2002).

17. G. Wang; P. Zhu; T. J. Marks; J. B. Ketterson, "Ultrafast Frequency-Selective Optical Switching Based on Thin Self-Assembled Organic Chromophoric Films with a Large Second-Order Nonlinear Response", *Appl. Phys. Lett.*, **81**, 2169-2171(2002).

18. P. M. Lundquist; W. Lin; H. Zhou; D. N. Hahn; S. Yitzchaik; T. J. Marks; G. K. Wong, "Frequency Doubling in Two-Component Self-Assembled Chromophoric Waveguide Structures", *Appl. Phys. Lett.*, **70**, 1941-1943(1997).

19. P. Zhu; M. E. van der Boom; H. Kang; G. Evmenenko; P. Dutta; T. J. Marks, "Realization of Expeditious Layer-by-Layer Siloxane-Based Self-assembly as an Efficient Route to Structurally Regular Acentric Superlattices with Large Electro-optic Responses", *Chem. Mater.,* **14**, 4982-4989(2002).

20. M. E. van der Boom; G. Evmenenko; P. Dutta; T. J. Marks, "Nanoscale Refractive Index Tuning of Siloxane-Based Self-Assembled Electro-Optic Superlattices", *Adv. Funct. Mater.*, **11**, 393-397(2001).

21. P. Wang; P. Zhu; W. Wu; H. Kang; C. Ye, "Design of Novel Nonlinear Optical Chromophores with Multiple Substitutions", *Phys. Chem. Chem. Phys.*, **1**, 3519-3525(1999).

22. M. Yang; B. Champagne, "Large Off-Diagonal Contribution to the Second-Order Optical Nonlinearities of ∧-Shaped Molecules", *J. Phys. Chem. A*, **107**, 3942-3951(2003).

23. B. Traber; J. J. Wolff; F. Rominger; T. Oeser; R. Gleiter; M. Goebel; R. Wortmann, "Hexasubstituted Donor-Acceptor Benzenes as Nonlinear Optically Active Molecules with Multiple Charge-Transfer Transitions", *Chem. Eur. J.*, **10**, 1227-1238(2004).

24. W.-J. Kuo; G.-H. Hsiue; R.-J. Jeng, "Novel Guest-Host NLO Poly(ether imide) Based on a Two-Dimensional Carbazole Chromophore with Sulfonyl Acceptors", *Macromolecules*, **34**, 2373-2384(2001).

25. H. Kang; P. Zhu; Y. Yang; A. Facchetti; T. J. Marks, "Self-Assembled Electro-Optic Thin Films with Remarkably Blue-Shifted Optical Absorption Based on an X-Shaped Chromophore", *J. Am. Chem. Soc.*, Submitted for publication.

26. M. Sigelle; R. Hierle, "Determination of the Electrooptic Coefficients of 3-Methyl-4-Nitropyridine 1-Oxide by an Interferometric Phase-Modulation Technique", *J. Appl. Phys.*, **52**, 4199-4204(1981).

27. D. Rafizadeh, and S.-T. Ho, "Numerical analysis of vectorial wave propagation in waveguides with arbitrary refractive index profiles", *Opt. Comm.* **141**, 17-20(1997).

28. R. G. Hunsperger, *Integrated Optics: Theory and Technology* (Springer, Berlin, Germany, 1995), Chaps 2 and 3.

29. C. C. Teng, and H. T. Man, "Simple Reflection Technique for Measuring the Electro-optic Coefficient of Poled Polymers", *Appl. Phys. Lett.*, **56**, 1734-1736(1990).